Performance Prediction and Flow Field Calculation for Airfoil Fan with Impeller Inlet Clearance

Shin-Hyoung Kang*, Renjing Cao
School of Mechanical and Aerospace Engineering, Seoul National University
Yangjun Zhang
Department of Mechanical Engineering, Tsinghwa University, China

The performance prediction of an airfoil fan using a commerical code, STAR/CD, is verified by comparing the calculated results with measured performance data and velocity fields of an airfoil fan. The effects of inlet tip clearance on performance are investigated. The calculations overestimate the pressure rise performance by about 10-25 percent. However, the performance reduction due to tip clearance is well predicted by numerical simulations. Main source of performance decrease is not only the slip factor but also impeller efficiency. The reduction in performance is 12-16 percent for 1 percent gap of the diameter. The calculated reductions in impeller efficiency and slip factor are also linearly proportional to the gap size. The span-wise distributions of phase averaged velocity and pressure at the impeller exit are strongly influenced by the radial gap size. The radial component of velocity and the flow angle increase over the passsage as the gap increases. The slip factor decreases and the loss increases with the gap size. The high velocity of leakage jet affects the impeller inlet and passage flows. With a larger clearance, the main stream moves to the impeller hub side and high loss region extends from the shroud to the hub.

Key Words : Performance, Airfoil Fan, Clearance

1. Introduction

Airfoil fans are widely used in a variety of applications for building ventilation and high flow rate air supply at plants with relatively lower pressure load. They generally cover the range of high specific speed. They are simple in structure, easy to manufacture, low cost in price, relatively highly efficienct and low noise. Since the fans are usually designed for various specifications based on a few designs using similarity rule, it is quite important to develop a highly efficient model. The efficiency of fans is affected by the impeller, inlet duct and volute. However, their effects are strongly coupled and difficult to separate. Computational Fluid Dynamics (CFD) techniques play an indispensable role in understanding the physical nature of the flow field. Therefore, CFD techniques are a powerful tool for design evaluation. The CFD techniques are mature enough to be used for fan design and to analyze the through flow. However, computer codes still need to be validated when they are used for a specific machine. Commercial codes also need validation since the solutions are dependent on grid alignment, boundary and initial conditions and turbulence model. One of the objectives of the present study is to verify the performance of STAR/CD by comparing against the measured performance data of airfoil fans.

On the other hand, there always exists a small gap between the rotating impeller and the fixed inlet casing. The static pressure is higher at the

* Corresponding Author,
E-mail : kangsh@snu.ac.kr
TEL : +82-2-880-7113 ; **FAX** : +82-2-883-0179
School of Meachanical and Aerospace Engineering., Seoul National. University, San 56-1, Shilim-dong, Kwanak-ku, Seoul, 151-742, Korea. (Manuscript **Received** october 7, 1998; **Revised** August 16, 1999)

discharge than that at the inlet, and there is leakage flow through the gap. The leakage is strongly dependent on the size of the gap, fan pressure rise and geometric configuration. The ratio of the leakage to the main flow rate determines the volumetric efficiency and is a parameter to increase the fan power. Several models have been proposed to estimate the volumetric efficiency in the past (Eck, 1976). However, the effects of gap and leakage flow on the impeller performance and the efficiency are not yet reported in the open literature. The high speed leakage flow will distort the impeller through flow and affect efficiency. The gap is not carefully controlled during manufacturing in the industry, especially for small size fans. It is quite interesting to investigate the gap effects on the impeller performance and the efficiency. Recent measurements of fan performance and impeller exit flow show considerable changes with gaps (Kang and Kim, 1998). The second objective of the present study is to numerically investigate the mechanism of performance and efficiency reduction due to the leakage flow through the gap. In this paper, the total performance of airfoil fan impeller with different radial clearances are presented, and the flow structure through the impeller are discussed.

2. Fan Model and Design Parametrs

2.1 Fan model

The airfoil fans are usually manufactured by forming and welding of thin plates for low cost and light weight. However, it is difficult to control the geometric surface accuracy. The impeller with twelve NACA65-810 blades is adopted in the present study. The NACA65-810 model was developed during a research project to develop a high efficiency model from the available models in production. The aluminum blades are wire-cut and imbedded on a machined plate hub as shown in Fig. 1. The machined shroud is fixed on to the blade tips. The dimensions of the fan are shown in Fig. 1. The tips of the inlet duct are also machined to eusure accurate circumferential gap distribution. The specifications are as follows:

Impeller diameter: 370 mm

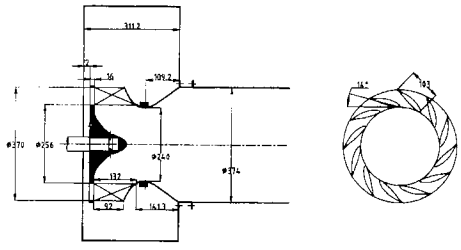

Fig. 1 Configuration of the airfoil fan

Number of blades: 12
Blade width at exit: 92.0 mm
Blade width at inlet: 132.0 mm
Chord length: 106 mm
Blade setting angle: 14 degree
Blade inlet angle: 33.5 degree
Blade exit angle: 24.6 degree

Other dimensions of the inlet duct and volute casing are presented in Fig. 1. Performance tests are carried out for three gap sizes; 1, 2 and 4 mm. Phase averaged velocity components and static pressure distributions are measured using a five hole Pitot tube at several impeller exit location. (Kim and Kang, 1998).

2.2 Important parameters

Several important non-dimensional parameters used in the present paper are as follows:

1) Total pressure coefficient :

$$\Delta\Psi = 2\Delta P_t / \rho U_2^2 \tag{1}$$

2) Flow coefficient:

$$\Phi = Q / \pi B D U_2 \tag{2}$$

3) Impeller efficiency:

$$\eta = \Delta P_t / \rho U_2 C_{\theta 2} \tag{3}$$

4) Total pressure loss coefficient:

$$\zeta = 2[U_2 C_{\theta 2} - (P_{t2} - P_{t1})/\rho] / U_2^2 \tag{4}$$

4) Rothalpy coefficient:

$$C_p^* = 2(P^* - P_1^*)/\rho U_2^2 \tag{5}$$

$$P^* = P + \rho(U^2 - W^2)/2 \tag{6}$$

5) Static pressure coefficient:

$$C_p = 2(P - P_1)/\rho U_2^2 \tag{7}$$

6) Slip factor:

$$\sigma = C_\theta / C_{\theta\infty} \tag{8}$$

Q, P, ρ denote the flow rate, pressure and density

respectively. U is the machine speed and C and W are the absolute and relative velocity components. D is the diameter. The subscript 1 and 2 denote the values at the inlet and exit of the impeller, respectively. P_1 is the mass averaged static pressure at the impeller inlet.

3. Calculation Method

3.1 Governing equations

The STAR/CD code, widely used in the many fluid machinery area, is adopted for the present study. The Reynolds-averaged Navier-Stokes equations and pressure linked continuity equation for incompressible and steady flow in a moving coordinate are solved using the Finite Volume Method. The standard form of $k-\varepsilon$ turbulence model is used for turbulence stress closure. The transport equation of turbulent kinetic energy and its dissipation rate are also solved.

3.2 Block and mesh generation

A program is developed to generate two pre-processing input data files for the STAR-CD, which include a VERTEX input data file and a SPLINE input data file. After loading these two input data files, the blocks can be generated using the mesh tool in the STAR-CD. The computational domain is comprised of five blocks. Blocks 1 and 2 represent the inlet duct and contraction part, and Block 3 is the rotating hub space of the impeller. Block 4 is the rotating impeller and 5 is the dummy parallel wall diffuser for specifying the exit boundary conditions.

A body-fitted grid is used and multiple rotating reference frames (implicit treatment) are adopted to model the rotation of the impeller (i. e. block 3 and 4 of rotating impeller with the same speed). This allows different mesh blocks with the model rotating at different speeds (i. e. easy treatment of the additional terms to the relevant equations dependent on the local angular velocity and the axis of rotation). The grid number for the cross section of each block has been selected to be 25×25 after several grid sensitivity tests.

Table 1 Calculated values of parameters with radial gaps at the design flow rate $\Phi=0.187$

c	0.0	2.6	5.0
Ψ_{Imp}	1.013	0.826	0.687
η_{Imp}	0.935	0.900	0.840
β_1	15.8	18.7	20.4
α_1	73.0	65.8	61.9
β_2	15.4	12.0	1.72
α_2	16.4	20.5	23.2
σ	0.80	0.72	0.67

3.3 Boundary conditions

Uniform inlet velocity is specified by the total flow rate. The turbulent kinetic energy and dissipation rate at the inlet are specified by the free stream turbulence intensity of 0.1 and a length scale of 0.01 D_1. D_1 is the inner diameter of the impeller. The conventional concept of wall function is used for both rotating and non-rotating surfaces. Since the through flow calculation is executed for a blade-to-blade space, there are periodic surfaces in Blocks 1, 2, 3 and 5, where cyclic boundary condition is used. On the rotating axis, symmetric boundary is assumed.

When there is a radial gap, inlet boundary conditions are imposed there. The magnitude of the leakage flow is determined as

$$V_{cl}=C\sqrt{2.0\Delta P/\rho} \tag{9}$$

where $C=1$, and ΔP is the fan static pressure rise. Since the flow distribution through the gap is not known, the magnitude and direction of velocity are assumed and their effects are investigated. Therefore, the magnitude of radial inlet flow velocity is assumed to be 28.8 m/s for the gap size of 2.6 and 5.0 mm. The results are summarized in Table 1.

4. Results and Discussions

4.1 Total performance

The fan's design flow rate is 0.698m^3/s at 1, 800rpm. Measured fan pressure rise, impeller efficiency, and slip factor for 2 and 4mm gaps (corresponding to $c/D_1=0.00781$ and 0.0156) are presented as solid symbols in Fig. 2. c and D_1

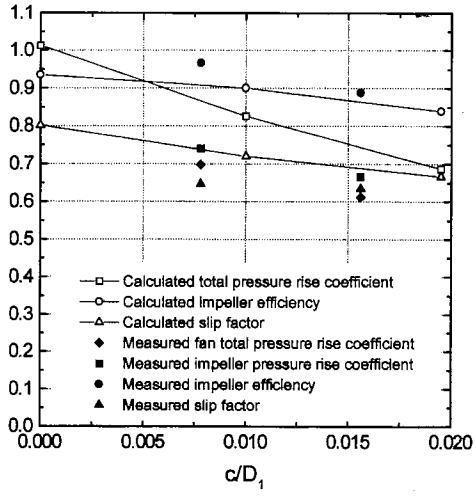

Fig. 2 Variations of calculated and measured performance parameters with the gap size

denote the radial gap size and the inner diameter of the impeller, respectively. Performance of the impeller were evaluated using the measured velocity and total pressure profiles at $\theta=270°$ of the volute (Kang and Kim, 1998). The difference between the fan and impeller total pressure coefficients is mainly due to the loss in the volute which, in this case, is about 0.05. The pressure rise of the fan decreases considerably as the gap size increases. If the rate of reduction is assumed to be a linear function of the gap size, the following relation is obtained.

$$\Delta\Psi_{Fan}/\Psi_{Fan}=14.2c/D_1 \tag{10}$$

$$\Delta\Psi_{Imp}/\Psi_{Imp}=11.9c/D_1 \tag{11}$$

The total pressure coefficient of the fan are 0.817, 0.718 and 0.627 for the values of 0.0, 0.01 and 0.0195 of c/D_1, where the performance are calculated for three radial clearances, i. e. 0.0, 2.6 and 5.0 mm. The calculated values of parameters are summarized in Table 1 and shown in Fig. 2 different gaps. Note that the corresponding non-dimensional values are 1.013, 0.826 and 0.687, respectively, and the following relation is obtained.

$$\Delta\Psi_{Imp}/\Psi_{Imp}=16.5c/D_1 \tag{12}$$

The calculations over-predict the pressure rise performance by about 10-25 percent. We should note that there are many sources of uncertainty for performance evaluation at the impeller exit and also for errors in numerical method and turbulence modeling. The difference in the configurations of the real flow and calculation models, (i. e. the additional pressure loss from the surface roughness and miss-alignment of the duct and impeller) are also important. However, it is difficult to control these variables for fans. Even though there are considerable differences between the measured and calculated values of the performance, it is interesting that the reduction rates of performance with gaps are quite well predicted by numerical simulations.

The main sources of performance decrease include not only the slip factor but also impeller efficiency. The reduction in performance is linearly proportional to the gap size-i. e. 12-16 percent reduction for 1 percent gap of the diameter. The calculated reductions in impeller efficiency and slip factor are also linearly proportional to the gap size. The contributions of the slip factor and viscous loss to the overall performance are dominant.

4.2 Averaged flow distribution at the impeller exit

The variations of design parameters can be investigated by observing the variations of velocity profiles and pressure distributions at the impeller exit including the flow angle α, radial velocity component C_{r2}/U_2, tangential velocity component $C_{\theta 2}/U_2$, local slip factor, and pressure coefficients C_p and C_{pt}. Figure 3 shows the distributions of absolute radial velocity component C_{r2}/U_2 normalized by the rotating velocity at the impeller exit. For the case without gap, C_{r2}/U_2 is nearly uniform over the 60 percent of the span. As the gap size increases, the radial velocity decreases from the hub region to the core and shows a local minimum. However, it increases again near the shroud. The trend of variation is the same as the measured one except on the shroud and hub surfaces, where the measured boundary layers are thicker. The variation of tangential component of absolute velocity, $C_{\theta 2}/U_2$ are shown in Fig. 4. The $C_{\theta 2}/U_2$ distribu-

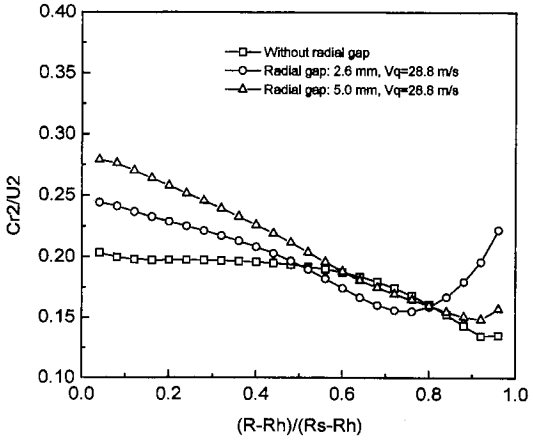

Fig. 3 Variations of radial component of velocity at the impeller exit

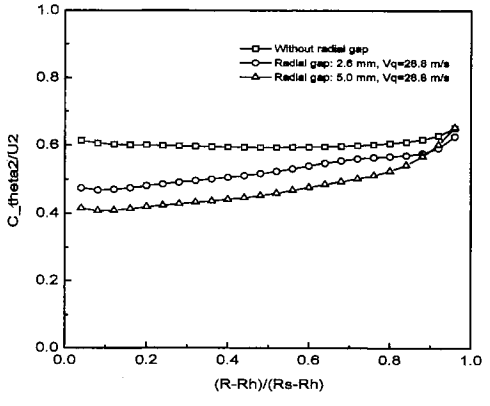

Fig. 4 Distributions of tangential component of velocity at the impeller exit

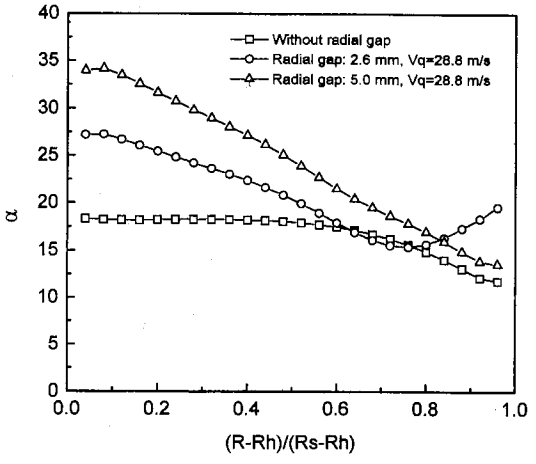

Fig. 5 Distributions of flow angle of absolute velocity at the impeller exit

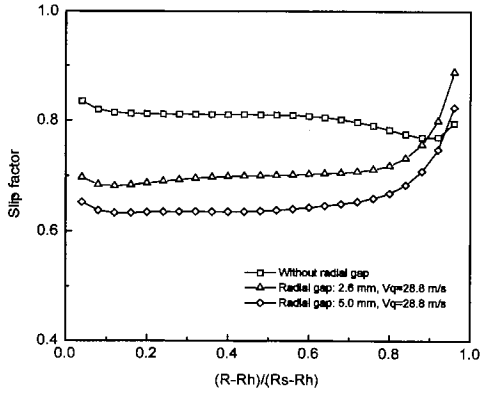

Fig. 6 Span-wise distributions of slip factor at the impeller exit

tion for each case is uniformly distributed through the span, however show small increases over the shroud in Fig. 4. As the gap size increases, the values of $C_{\theta 2}/U_2$ becomes smaller over the span. Thus, the decrease in the tangential momentum exchanges and slip factor in the sequel. Figure 5 shows the distributions of absolute flow angle from the hub to shroud. The leakage flow makes the flow more radial due to the increase in the radial component of velocity over the hub. The leakage flow generally pushes the main flow to the hub side, increases the radial component, decreases the tangential component and larger flow angle over the hub. This makes the flow over the shroud changes steeply and generates extra stream-wise vorticity. Slip factors shown in Fig. 6 are influenced by the clearance gap just as the tangential velocity components.

Figure 7 shows the distributions of static pressure coefficients C_p, which decreases from the hub to shroud. The value of C_p is the highest when there is no gap. The total pressure coefficient C_{pt} distributions at the impeller exit are shown in Fig. 8. the C_{pt} distribution is related to the pressure loss of the impeller. For zero clearance, the C_{pt} is nearly constant from the hub to shroud and has its maximum value. The clearance flow generates shear vorticity and distorts the through flow downstream and increase the viscous loss. For larger gap, the values of C_{pt} are smaller from the impeller hub to shroud. The total pressure loss

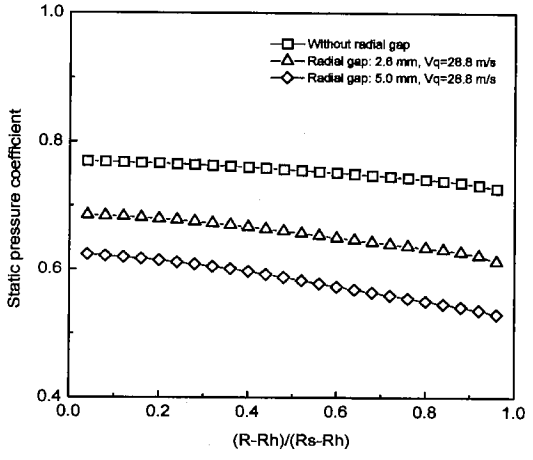

Fig. 7 Span-wise distributions of static pressure at the impeller exit

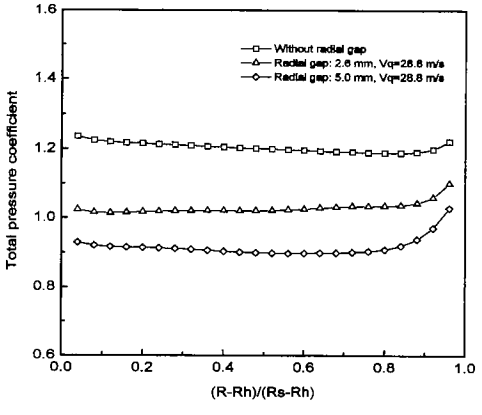

Fig. 8 Distributions of total pressure coefficient at the impeller exit

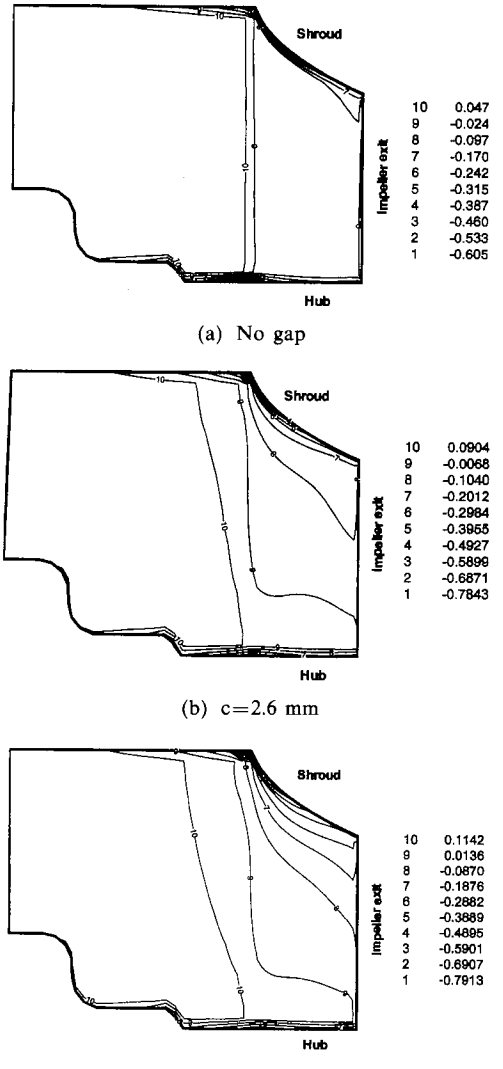

Fig. 9 Averaged rothalpy coefficient contours of the fan at design condition

increases as the gap and the clearance velocity increase. The changes in the flow at the impeller exit explain the mechanism of reduction in the slip factor and efficiency with the tip clearance.

4.3 Flow structure

The blade-to-blade relative flow field is investigated. The tip leakage flow pushes the main inlet flow to have higher inlet flow angle and relative velocity near the leading edge on the suction surface. On the other hand, a thicken boundary layer zone appears over the trailing edge of the suction surface as the radial gap increases. Tangentially averaged static pressures show that they are uniformly distributed from hub to shroud. However, they are distorted near the shroud inlet due to the high leakage velocity and show a lower pressure region there. Such flow distortion due to the leakage flow can be observed in the rothalpy distributions shown in Figs. 9 (a) to (c). They are constant through the rotating impeller for an ideal case, and their variations show viscous losses. The viscous losses are concentrated at the shroud and hub surfaces where boundary layers develop. The region of lower P^* develops from the impeller inlet to the exit and expands through the impeller passage as

the gap size increases as shown in Figs. 9. This is one of the sources influencing the total performance reduction of the impeller. The main flow structure inside the impeller is changed due to the clearance flow and the low P^* near the impeller shroud is due to the slit flow as well as its strong mixing effect with the main flow.

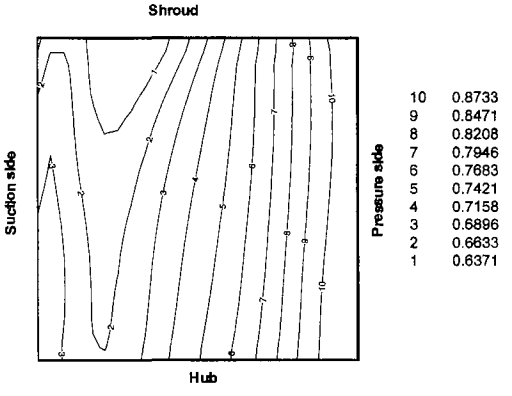

(a) no gap

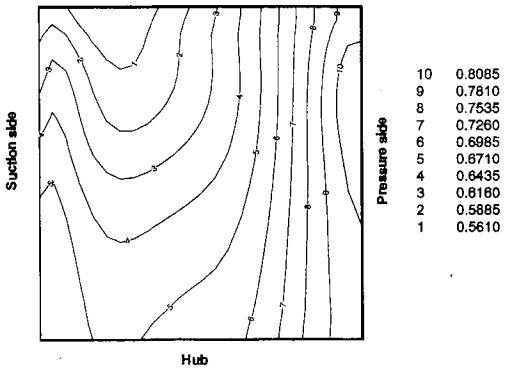

(b) c=2.6 mm

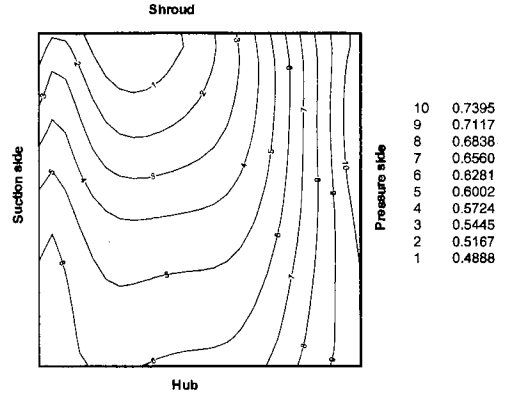

(c) c=5.0 mm

Fig. 10 Static pressure coefficient contours of the fan at the impeller exit.

The flow structure at the impeller exit plane is investigated in more detail. The static pressure coefficient contours at the impeller exit for different gaps are shown in Figs. 10. In Fig. 10(a), the static pressure coefficient near the pressure side is generally higher than that on the suction side. The uniform static pressure distribution from hub to shroud is shown. except the concentrated low pressure region over the suction/shroud corner, which is usually known as the jet-wake structure. However, the uniform static pressure distribution is distorted, as shown in Figs. 10 (b) and (c), as the gap size increases. The region of low static pressure extends to the hub and pressure sides. It occupies almost 2/3 in the pitch and span wise direction, respectively, for the 5.0mm gap.

The total pressure coefficient contours at the impeller exit for various clearances are shown in Figs. 11(a), (b) and (c). The result presented in Fig. 11(a) for the impeller without gap shows that the total pressure coefficient near the suction and pressure sides are higher than that over the inner core region. The highest total pressure coefficients appear at the suction/pressure and shroud/hub corners, and the span-wise variation is generally small. When the radial clearance is 2. 6mm, Fig. 11(b) shows that the region with lower pressure becomes large. Figure 11(c) for 5.0mm radial clearance shows that the low pressure region extends over the large portion of the impeller passage. The highest pressure rise is observed in the pressure-shroud corner for all the cases.

The rothalpy coefficient contours at the impeller exit for various clearances are shown in Figs. 12(a), (b) and (c). The low C_p^* region is located near the corner suction/shroud corner and extends its size to the core region as the gap size increases. This result is due to the thick boundary layer and strong vortex flow developed there. The light C_p^* region is located near the pressure/hub corner diagonally opposite to the low corner C_p^* region.

The distributions of total pressure loss coefficient for the three cases are shown in Figs. 13(a), (b) and (c), respectively. The main loss sources

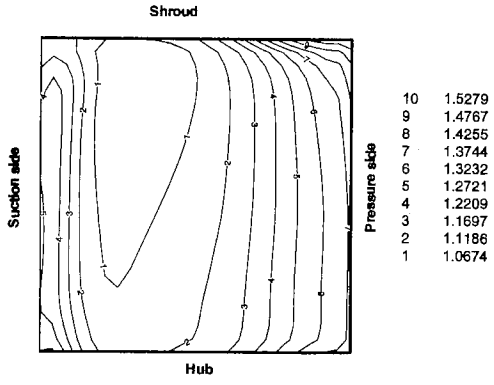

(a) No gap

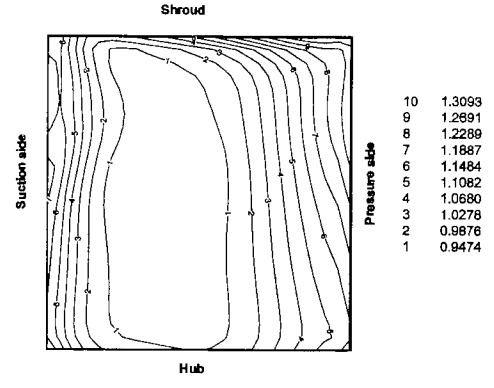

(b) c=2.6 mm

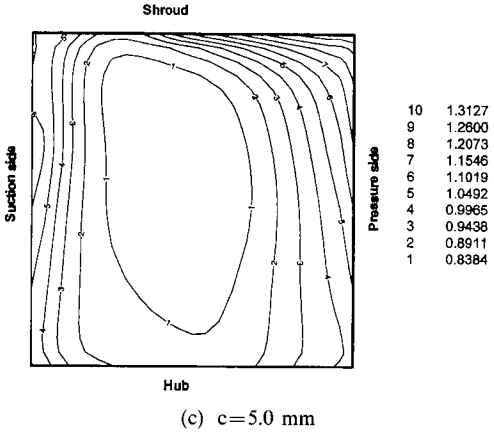

(c) c=5.0 mm

Fig. 11 Total pressure coefficient contours of the fan at the impeller exit.

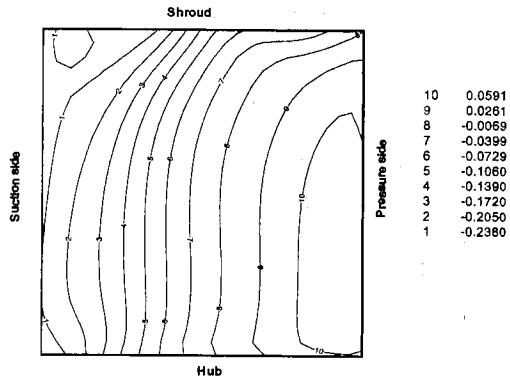

(a) No gap

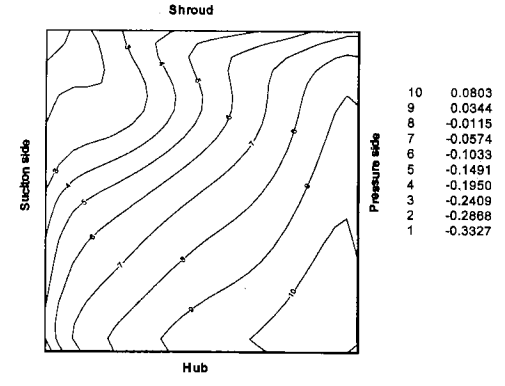

(b) c=2.6 mm

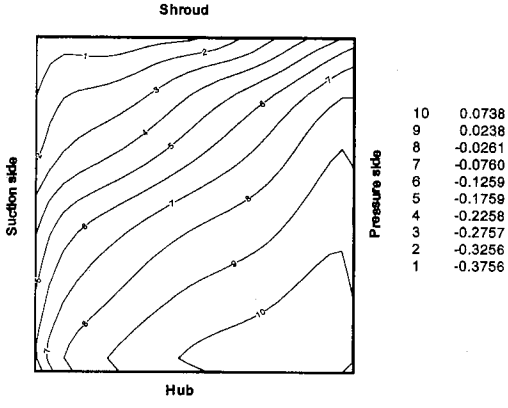

(c) c=5.0 mm

Fig. 12 Rothaply coefficient contours of the fan at the impeller exit.

consist of the viscous loss due to the blade boundary layer development, formation of secondary flow, and their interaction with the main flow. The locations of the maximum loss are over the suction/shroud region, not on the corner.

Finally the slip factor distribution, is presented in Fig. 14. Since the flow is well guided near the pressure surface, the slip factor is large there. It is small over the shroud/suction corner for the zero gap, as shown in Fig. 14(a). It is interesting to

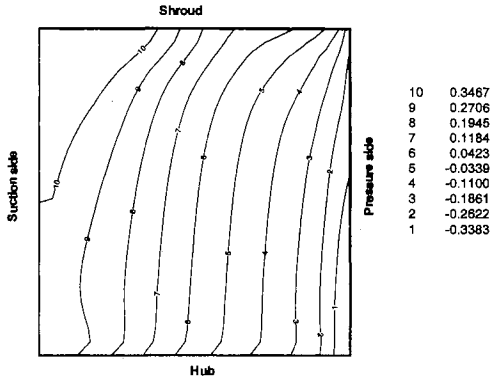

(a) No gap

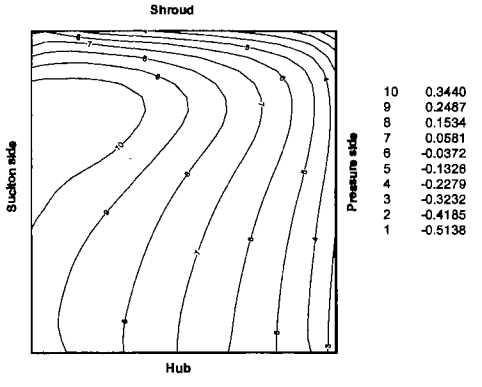

(b) c=2.6 mm

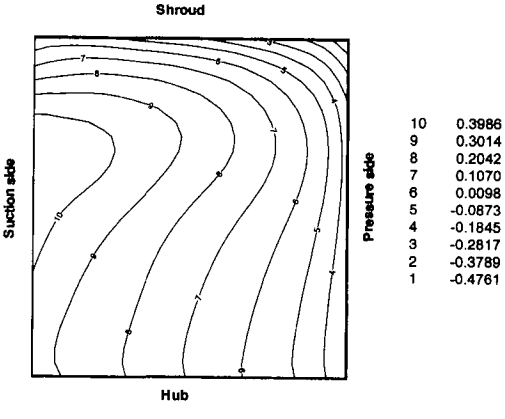

(c) c=5.0 mm

Fig. 13 Total pressure loss coefficient contours of the fan at the impeller exit.

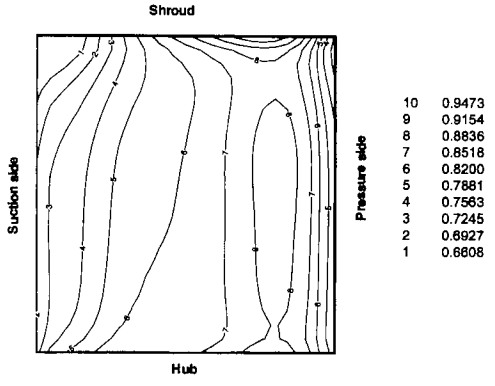

(a) No gap

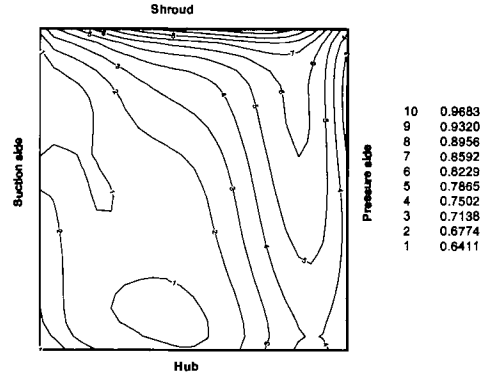

(b) c=2.6 mm

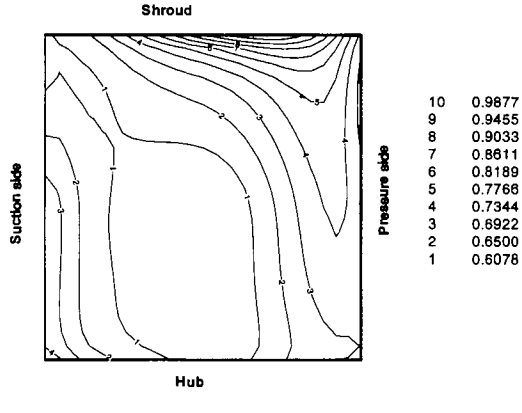

(c) c=5.0 mm

Fig. 14 Slip factor contours of the fan at the impeller exit.

note that the span-wise variation is small and the highest slip factor is observed over the shroud. As the radial clearance increases to 2.6mm, Fig. 14 (b) shows that the region of higher slip factor becomes smaller and moves to the shroud, where the large values appear over the shroud. This corresponds to the span-wise variation presented in Fig. 6. The region of small slip factor occupies more than half the impeller passage. When the radial clearance is 5.0mm, as shown in Fig. 14(c),

the slip factor distribution becomes more non-uniform and the region of low slip factor is enlarged and moves to the pressure side. The high slip factor region is also observed over shroud. However, the value becomes small.

5. Conclusions

The through flow of the airfoil fan impeller is numerically simulated and the effects of the impeller gap size on the pressure rise performance, slip factor, and losses are investigated. The main conclusions are as follows:

(1) The total pressure rise coefficient and impeller efficiency decrease as the radial clearance gap increases. These reductions are mainly due to the decrease in the slip factor and increase in the viscous loss of the through flow.

(2) The span-wise distributions of the phase averaged velocity, flow angle, and pressure at the impeller exit are strongly influenced by the radial gap size. The radial component of velocity and the flow angle increase as the gap increases, except near the shroud region.

(3) The high velocity of the leakage flow in jet form distorts the impeller inlet flow and the impeller passage flow. With a bigger clearance gap, the main stream moves to the impeller hub side and the high loss region extends from the shroud to the hub.

Acknowledgement

This study was supported by Century Co. Ltd. and Turbo and Power Machinery Research Center in 1998.

References

Eck, B., 1973, *Fans*, Pergamon Press, Oxford.

Kang, S. H. and Kim Y. J., 1998, Effects of the Impeller Inlet Tip Clearance on the Flow and Performance of Airfoil Fans, TML MS-5, Seoul N. University.